



Review:

Review of optical tweezers in vacuum*

Nan LI[†], Xun-min ZHU, Wen-qiang LI, Zhen-hai FU, Meng-zhu HU, Hui-zhu HU^{†‡}

State Key Laboratory of Modern Optical Instrumentation, College of Optical Science and Engineering,
 Zhejiang University, Hangzhou 310027, China

[†]E-mail: nanli@zju.edu.cn; huhuizhu2000@zju.edu.cn

Received Feb. 23, 2019; Revision accepted May 9, 2019; Crosschecked May 27, 2019

Abstract: As a versatile tool for trapping and manipulating neutral particles, optical tweezers have been studied in a broad range of fields such as molecular biology, nanotechnology, and experimentally physics since Arthur Ashkin pioneered the field in the early 1970s. By levitating the “sensor” with a laser beam instead of adhering it to solid components, excellent environmental decoupling is achieved. Furthermore, unlike levitating particles in liquid or air, optical tweezers operating in vacuum are isolated from environmental thermal noise, thus eliminating the primary source of dissipation present for most inertial sensors. This attracted great attention in both fundamental and applied physics. In this paper we review the history and the basic concepts of optical tweezers in vacuum and provide an overall understanding of the field.

Key words: Optical tweezers; Optical trapping in vacuum; Optical cooling

<https://doi.org/10.1631/FITEE.1900095>

CLC number: O436

1 Introduction

Radiation pressure is a direct demonstration of the momentum carried by electromagnetic waves. It was first proposed in 1619 by Johannes Kepler that light radiated from the Sun could explain the phenomenon that a comet’s tail always points away from the Sun (Kepler, 1619).

In 1862, Maxwell worked out the mathematical framework of electricity and magnetism, suggesting that electromagnetic radiation has momentum, which was then proved experimentally by Russian physicist Pyotr Lebedev (Lebedev et al., 1901) and by Nichols and Hull (1903) separately at the dawn of the 20th century. The invention of the laser by Townes in 1960

provided a critical technology for optical trapping and manipulation (Townes, 1999).

Ashkin has been considered as the father of optical tweezers. In 1970, using a focused beam, Ashkin managed to control the dynamics of low-absorption silica particles (Ashkin, 1970). In this work, he identified two components of radiation force: a scattering force along the axis of the laser and a gradient force along the direction of the laser intensity gradient. It was also predicted that this mechanism applies for neutral atom trapping. One year later, Ashkin successfully trapped 20- μm glass spheres in air and vacuum at pressures around ~ 1 Torr (1 Torr ≈ 133.322 Pa) (Ashkin and Dziedzic, 1971) and indicated that if the viscous damping can be further reduced, namely trapping particles in a high vacuum environment, extremely low dissipation is possible and the measurement sensitivity would have great potential for improvement. Ashkin and his colleagues reported trapping of oil droplets in vacuum down to $\sim 10^{-6}$ Torr in 1975 (Ashkin and Dziedzic, 1976). This is the first setup of an optical trap in a high vacuum environment. In 1986, Ashkin reported a technique for trapping micron-scale dielectric particles using a single tightly

[‡] Corresponding author

* Project supported by the Joint Fund of Ministry of Education, China (No. 6141A02011604), the Fundamental Research Funds for the Central Universities, China (Nos. 2016XZZX00401 and 2018FZA5002), and the National Program for Special Support of Top-Notch Young Professionals, China

ORCID: Nan LI, <https://orcid.org/0000-0003-3585-2273>; Hui-zhu HU, <https://orcid.org/0000-0003-1690-9414>

© Zhejiang University and Springer-Verlag GmbH Germany, part of Springer Nature 2019

focused laser beam, a technology which is now commonly referred to as “optical tweezers” (Ashkin et al., 1986).

Since the early 1990s, optical trapping and manipulation have been widely studied in biological sciences, starting by trapping an individual tobacco mosaic virus (Ashkin et al., 1990). After that, many groups began to use optical force spectroscopy to characterize the mechanical properties of biomolecules and biological motors (Ashkin et al., 1990; Block et al., 1990; Bustamante et al., 1994). Optical tweezers allowed biophysicists to observe the forces and dynamics at the single molecule level, leading to a greater understanding of biochemical processes. In 2018, the Nobel Prize in Physics was awarded “for groundbreaking inventions in the field of laser physics” with one half to Ashkin “for the optical tweezers and their application to biological systems” (<https://www.nobelprize.org/prizes/physics/2018/press-release/>).

Remarkable progress in trapping micro-scale and nanoscale spheres at high vacuum pressures was achieved by Li and Novotny, respectively. In 2010, Li et al. reported the measurement of the instantaneous velocity of a Brownian particle with counter propagating dual-beam optical tweezers (Li et al., 2010, 2011). Gieseler et al. (2012) managed to cool its three spatial degrees of freedom by means of an active parametric feedback scheme and reported an optically trapped nanoparticle in high vacuum. These works indicated that, as a system couples optical field and mechanical oscillator, optical trapped particles in vacuum could be an ideal candidate for precision measurement, pushing the frontiers of sensitivity in an accelerometer (Monteiro et al., 2017), a force sensor (Ranjit et al., 2016), and so on (Moore et al., 2014; Hoang et al., 2016). In addition, it paves the way for generating a macroscopic quantum state when the particles are cooled to the quantum ground state (Park and Wang, 2009; Rocheleau et al., 2010; Chan et al., 2011; Teufel et al., 2011). The creation of “Schrödinger cats,” quantum superposition of macroscopic observables, and the study of their destruction by decoherence, are especially fascinating because they might provide a better understanding of the transition from the classical to the quantum world. Since then, optical trapping in vacuum has received significant attention and achieved rapid technological

development. An increasing number of groups are involved in this intriguing field.

In recent years, there have been many reviews concerning optical tweezers. A comprehensive introduction for optical force calculation or simulation in optical tweezers has been published (Nieminen et al., 2014; Bui et al., 2017; Sukhov and Dogariu, 2017; Polimeno et al., 2018), as well as reviews focusing on experiments and applications. Ciminelli et al. (2017) reviewed the state-of-the-art of nanotweezers proposed for trapping at the sub-micrometer nanoscale, especially the performance obtained with photonic and plasmonic nanotweezers. Gong et al. (2018) introduced the principles, technical details, and applications of optical trapping and manipulation of single particles in air. The most recent review by Gouesbet (2019) gave an overall understanding of generalized Lorenz-Mie theories and mechanical effects of laser light. This review focuses on the optical trapping of particles in vacuum, especially of those studies that concentrate on precision measurement. We start from the fundamental concepts of optical trapping, cooling, and detection. More detailed theoretical consideration could be found in Ashkin (2000), Grier (2003), Dienerowitz et al. (2008), Juan et al. (2011), and Maragò et al. (2013). In Section 3, the experimental system will be briefly introduced. Section 4 highlights several applications for this system.

2 Principle of optical trapping in vacuum

2.1 Optical trapping

Optical trapping is a consequence of radiation force which originates from the conservation of electromagnetic momentum. Through the exchange of momentum between light and particles, we may understand the forces that enable the stable confinement and manipulation of particles within optical traps. As Ashkin (1970) first illustrated in a seminal paper with an intuitive “back of the envelope” calculation, the acceleration experienced by a particle (1- μm fused silica) when interacted with a laser beam (1 W, focused to 1 μm) could be up to 10^8g . It suggested that the focused laser beam can be used to overcome the effect of Earth’s gravity on particles. Since then more detailed theoretical work on radiation force calculation was accomplished (Bohren and Huffman, 1983;

Ashkin et al., 1986; Neuman and Block, 2004; Juan et al., 2011). In this review we are going to briefly introduce the calculation methods. Readers may refer to the references mentioned above for more details.

As is known to all, light exerted a “scattering force” in the direction of beam propagation (the axial direction) and a “gradient force” towards the center of the beam (radial direction), where the light intensity is highest. There are mainly three kinds of frequently used approaches for computing radiation force depending on the size of the particle: geometrical optics, Rayleigh approximation, and the intermediate regime. The geometrical optics theory can fully agree with experiments only with a range of particle size greater than 10 times wavelength. Rayleigh approximation maintains validity only within the size range smaller than one tenth of a wavelength. As for the particles whose sizes fall within the intermediate scale (usually $0.1\lambda_0 \leq r \leq 10\lambda_0$, where λ_0 is the wavelength), the intermediate regime has to be used, including generalized Lorenz-Mie theory (GLMT), extended boundary condition method (EBCM), discrete dipole approximation (DDA), and numerical calculation methods that fall into two groups: finite element methods (FEM), finite difference methods such as finite difference time-domain method (FDTD) and finite difference frequency-domain method (FDFD) (Bui et al., 2017).

Although the intermediate regime works relatively poorly with memory and time outside the range of the intermediate scale compared with geometrical optics and Rayleigh approximation, it does offer enough accuracy over the whole scale. GLMT, EBCM, and DDA are all methods of calculating the T-matrix of the particle (Gouesbet, 2010; Gouesbet and Lock, 2015). The point-matching method is another way of calculating the T-matrix and is widely adopted in study of optical tweezers (Loke et al., 2001; Nieminen et al., 2003a). GLMT is too complex when the particle is not a uniform isotropic sphere. EBCM and DDA are more feasible ways in that case. EBCM supports a larger size of particle than DDA while losing its advantage in particle structure complexity. EBCM has been standardized so much for T-matrix nowadays that some just regard it as the T-matrix method. That is a wrong and discredited notion (Gouesbet, 2010). Once the T-matrix has been attained, it can be repeatedly used in calculation for

different conditions of illumination by monochromatic light (Gouesbet and Gréhan, 2017). Those conditions are widely present in particle movement modeling of optical tweezers. The entire calculation must be restarted in numerical calculation methods. Thus, they are more suitable for static analysis in quite complex particle structures rather than dynamic modeling. In Table 1, we list all three kinds of regimes. We then outline the principles.

Table 1 Three kinds of regimes used for computing radiation force

Particle size	Regime	Reference
$r \geq 10\lambda$	Geometrical optics	Ashkin (1992)
$r \leq 1/10\lambda$	Rayleigh approximation	Harada and Asakura (1996)
$1/10\lambda < r < 10\lambda$	Intermediate regime	GLMT (Ren et al., 1996) EBCM (Waterman, 1965, 1971) DDA (Nieminen et al., 2001; Mackowski, 2002) FEM (White, 2000) FDTD (Gauthier, 2005)

2.1.1 Geometrical/Ray optics regime

This intuitive and simple approach has been proven to be successful, for example, in demonstrating radiation forces acting on cells (Chang et al., 2006), the deformation of microscopic bubbles in an optical field (Skelton et al., 2012), the optical lift effect (Swartzlander et al., 2010), and the emergence of negative optical forces (Kajorndejnkul et al., 2013). Incident rays are split into the reflected and transmitted rays on the surface of the particle, and the direction difference between them entails a change of momentum according to the action-reaction law. Ray optics traces the optical rays in the particle and sums the change of momentum up to compute the forces acting on the particle. The surface reflection depends on the relative refractive index of the particle and the medium, and it is closely related to the scattering force. Thus, it is more difficult to trap particles in air than in water (Wright et al., 1994). A complete MATLAB software package, Optical Tweezers in Geometrical Optics (OTGO), has been developed by Callegari et al. (2015), to perform the calculation of optical forces and torques within the geometrical optics approach.

2.1.2 Rayleigh regime

Rayleigh approximation has been extensively employed for the calculation of radiation force exerted on nanoparticles. Rayleigh approximation treats a nanoparticle as a dipole and derives analytical solutions. The scattering force and gradient force of a laser beam on a nanosphere are given by Harada and Asakura (1996):

$$\begin{cases} \mathbf{F}_{\text{scat}}(\mathbf{r}) = \hat{z} \frac{128\pi^5 R^6}{3c\lambda_0^4} \left(\frac{m^2 - 1}{m^2 + 2} \right)^2 n_{\text{med}}^5 I(\mathbf{r}), \\ \mathbf{F}_{\text{grad}}(\mathbf{r}) = \frac{2\pi n_{\text{med}} R^3}{c} \left(\frac{m^2 - 1}{m^2 + 2} \right) \nabla I(\mathbf{r}), \end{cases} \quad (1)$$

where \hat{z} is the unit vector on the z axis and is also the direction of beam propagation. c is the speed of the laser light in vacuum and λ_0 is the wavelength of the laser in vacuum. R is the radius of the nanosphere. m is the relative refractive index of the particle and the medium. n_{med} is the refractive index of the medium. Lastly, $I(\mathbf{r})$ means the light intensity at the coordinate \mathbf{r} . The scattering force is proportional to R^6 while the gradient force is proportional to R^3 . Therefore, trapping larger particles turns out to be more difficult because the scattering force increases much faster than the gradient force as the size of the nanosphere increases (Li et al., 2011). In experiment, particles with radius up to 170 nm can be trapped in a single tightly focused beam configuration (Ahn et al., 2018).

2.1.3 Intermediate regime

Only GLMT is given as an example here since it is relatively convenient to understand in various methods of the intermediate regime. Bromwich scalar potentials U_{TM} and U_{TE} are originally used in GLMT to express the incident, the scattered, and the internal (or sphere) waves. TM means transverse magnetic and transverse electric is abbreviated to TE. For instance, according to Gouesbet et al. (1988), the Bromwich scalar potentials for the incident wave read as

$$\begin{cases} U_{\text{TM}}^i = \frac{E_0}{k} \sum_{n=1}^{\infty} \sum_{m=-n}^{+n} c_n^{p^w} g_{n,\text{TM}}^m \psi_n(kr) P_n^{|m|} \cos\theta \exp(im\varphi), \\ U_{\text{TE}}^i = \frac{H_0}{k} \sum_{n=1}^{\infty} \sum_{m=-n}^{+n} c_n^{p^w} g_{n,\text{TE}}^m \psi_n(kr) P_n^{|m|} \cos\theta \exp(im\varphi), \end{cases} \quad (2)$$

in which the superscript “i” designates “incident.” E_0 is associated with electric field amplitude and k is the wave-number. $g_{n,\text{TM}}^m$ and $g_{n,\text{TE}}^m$ are the beam shape coefficients. $\psi_n(kr)$ belongs to spherical Bessel functions. The other parts of Eq. (2) are fixed functions of their superscript, subscript, and variables in brackets. Results in the above scalar framework can be converted to a vectorial version in terms of regular vector spherical wave functions (regular VSWFs) to obtain T-matrix from GLMT. The incident and scattered fields are written as linear combinations of regular VSWFs (Nieminen et al., 2003b):

$$\begin{cases} E_{\text{incident}}(\mathbf{r}) = \sum_{n=1}^{\infty} \sum_{m=-n}^n a_{nm} \text{Rg}M_{nm}(kr) + b_{nm} \text{Rg}N_{nm}(kr), \\ E_{\text{scattered}}(\mathbf{r}) = \sum_{n=1}^{\infty} \sum_{m=-n}^n p_{nm} \text{Rg}M_{nm}(kr) + q_{nm} \text{Rg}N_{nm}(kr), \end{cases} \quad (3)$$

where $\text{Rg}M_{nm}(kr)$ and $\text{Rg}N_{nm}(kr)$ are regular VSWFs and they are a complete set of solutions to the vector Helmholtz equation. a_{nm} and b_{nm} are expansion coefficients of the incident field. p_{nm} and q_{nm} are expansion coefficients of the scattered field. a_{nm} and b_{nm} can be written as a vector noted as \mathbf{A} . Vector \mathbf{P} is noted for p_{nm} and q_{nm} . Their relationship can be expressed in matrix form as

$$\mathbf{P} = \mathbf{T}\mathbf{A}, \quad (4)$$

where \mathbf{T} is exactly the T-matrix. If the electromagnetic properties of the particle are linear and isotropic, the T-matrix depends only on the particle itself (its composition, size, shape, and orientation) and is independent of the incident field. That testifies to the reuse of the T-matrix for different conditions of illumination by monochromatic light as mentioned above. There is a computational toolbox developed by Nieminen et al. (2007) adopting the EBCM and point-matching method to obtain numerical results of the optical forces.

2.2 Optical cooling

Ashkin demonstrated that a laser beam can be a powerful tool for trapping and manipulating dielectric particles, and for feedback cooling (Ashkin and Dziedzic, 1977). Hänsch and Schawlow (1975) and

Wineland and Dehmelt (1975) first pointed out the possibility of using it for neutral atom cooling. Subsequently, cold atoms were experimentally realized by Chu et al. (1985); since then laser cooling became an extraordinary technique, enabling many applications including the atomic clock (Ludlow et al., 2015), Bose-Einstein condensation (BEC) realization (Davis et al., 1995), and quantum precision measurement (Peters et al., 2001; Appel et al., 2009).

When trying to trap a dielectric particle in high vacuum, optical cooling of center-of-mass (COM) motion turns out to be an essential and critical process. For micro- and nanoscale particles, radiation pressure plays a vital role in cooling by dissipating the kinetic energy (Braginskii and Manukin, 1967; Braginskii et al., 1970). The first experimental demonstration of this proposal was achieved by Cohadon et al. (1999), where they cooled the vibrational modes of a macroscopic end mirror. Now feedback cooling of particles is a quite mature technique, which will be outlined in the following. It should be emphasized that laser cooling neutral atoms is different from laser cooling dielectric particles. Unlike using atomic internal degrees of freedom (Lett et al., 1988), cooling dielectric particles in optical tweezers deals with external degrees of freedom.

The harmonic oscillator model is typically used to characterize the dynamic properties of the trapped particle in air. Therefore, the power spectral density (PSD) of COM displacement of the particle has a Lorentzian curve (Kirstine and Henrik, 2004):

$$\begin{cases} S_x(\omega) = \frac{k_B T}{M \Omega^2} f_s(\omega), \\ f_s(\omega) = \frac{\Gamma_0 \Omega^2}{(\Omega^2 - \omega^2)^2 + \omega^2 \Gamma_0^2}, \end{cases} \quad (5)$$

where $f_s(\omega)$ is the normalized Lorentzian function. Γ_0 indicates the damping coefficient in air. $\Omega = (k/m)^{1/2}$ is the free oscillation angular frequency, in which k is the stiffness of the optical tweezers and M is the mass. k_B is the Boltzmann constant and T is the environmental temperature. The linearized incompressible time-dependent Navier-Stokes equation can describe the motion of particles trapped in liquid. This is similar to the harmonic oscillator model (Clercx and Schram, 1992). According to the Wiener-Khinchin theorem (Cohen, 1998), the root mean square (RMS)

of the displacement and velocity of the particle COM are

$$\begin{cases} \sqrt{\langle x^2 \rangle} = \sqrt{\int_{-\infty}^{+\infty} S_x(\omega) d\omega} = \sqrt{k_B T / k}, \\ \sqrt{\langle v^2 \rangle} = \sqrt{\int_{-\infty}^{+\infty} \omega^2 S_x(\omega) d\omega} = \sqrt{k_B T / M}. \end{cases} \quad (6)$$

Thus, the average kinetic energy of the particle is $\langle Mv^2/2 \rangle = k_B T/2$, which exactly agrees with the equipartition theorem.

The damping coefficient decreases, and thus the quality factor Q ($Q = \Gamma_0 / \Omega$) increases, as air pressure drops. This means the motion of the COM of the particle becomes closer to simple ideal harmonic motion. As shown in Eq. (6), $\langle x^2 \rangle$ depends only on T and k , so it does not change with air pressure. The consequence is that at low air pressure the oscillation will be magnified at the angular frequency, while motion at other frequency bands will be compressed. This is of great significance for the application of optical tweezers in low-frequency precision measurement. On the other hand, the influence of external noise caused by Brownian motion is largely eliminated in vacuum, giving rise to high measurement accuracy far exceeding conventional means. However, intensified Brownian motion and a laser heating effect at extremely low pressure would reduce the survival time of the particle so much that it usually escapes in several seconds or even shorter time without an additional strategy. Therefore, the displacement RMS of the particle must be effectively suppressed, which is commonly referred to as COM cooling. Generally speaking, COM cooling could be understood as a procedure of damping the motion with radiation pressure. Several commonly used cooling methods in vacuum optical tweezers system will be introduced in Section 3.3.

The PSD of particle displacement in the low frequency range decreases only when air pressure drops, demonstrated by the red line and green line in Fig. 1. Particles under green line conditions are more likely to escape due to lack of cooling in a low-pressure environment as mentioned in the previous paragraph.

Although the laser can be used for cooling the particles (COM motion cooling), it also brings heating mechanisms since intense laser light is tightly focused to intensities of MW/cm² in order to apply

forces to a submicron particle. Even though it is essential to choose material which is almost “transparent” (extremely low absorption efficiency) to the trapping laser, the heating due to partial absorption does exist, which leads to radiation forces that reduce the trap stability. Many groups have studied this nonnegligible problem theoretically and experimentally (Peterman et al., 2003; Mao et al., 2005; Catalá et al., 2017).

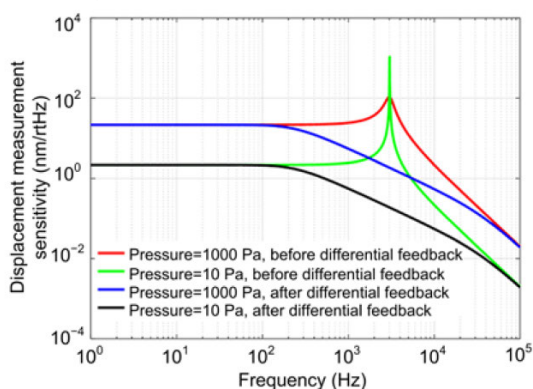


Fig. 1 Simulation of the PSD of particle displacement with differential cooling and air pressure reducing conditions

The particle trapped with dual beams is a microsphere of diameter 10 μm . The optical power of each laser beam is 150 mW and the NA of each lens is 0.35. References to color refer to the online version of this figure

3 Experimental scheme

Optical trapping of a microsphere in air or even in vacuum is much more challenging than optical trapping a microsphere in liquid. The first problem one may encounter is launching. Unlike the circumstance in liquid, it requires ultrahigh acceleration ($\sim 10^4 g$) to realize detachment between the particles and the substrate in air. Considering stable capturing in vacuum, precise displacement detection and cooling process are critical. In this section we will review the above key techniques in a vacuum optical tweezers system.

3.1 Launch

In liquid, the suspended particle near the trap could be easily captured because its buoyancy would counteract the gravity in the vertical direction. However, in air or vacuum, the particles need to be detached from the storage medium, and the initial

capture process can be achieved after it enters the effective region of the optical trap (Fu et al., 2018b). The scope of the optical trap is limited. Thus, the initial capture process requires the particle enter the light field at a suitable rate.

The particle sample would inevitably adhere to the surface of the substrate of glass slide because of the strong adhesion force. Therefore, in previous research on fundamental physics, two conventional methods for initial particle loading were proposed: piezo and nebulizer. The high-frequency vibration of piezoelectric ceramic can separate the particles from the surface of the substrate. This is generally applicable to micron-sized dielectric particles (Butts, 2008; Li et al., 2010, 2011; Arita et al., 2013; Ranjit et al., 2015) (Fig. 2a). Ashkin in his pioneering experiments used a piezo-electric transducer to achieve initial particle loading (Ashkin and Dziedzic, 1971; Ashkin and Dziedzic, 1976). The adhesion force is inversely proportional to the square of particle diameter, which means that there is a minimum particle size that can be separated for an acceleration provided by the piezo. For the initial loading of smaller nanoparticles, one needs to use an ultrasonic nebulizer (Summers et al., 2008; Grass, 2013; Kiesel et al., 2013; Gieseler, 2014; Millen et al., 2014). A highly diluted solution of the sample can be broken into small droplets by an ultrasonic nebulizer, and then nanoparticles sprayed into the free space would be captured after the solution component of droplets evaporates. Therefore, a highly volatile solution such as propanol was mostly used in this method, and the solution components can be quickly volatilized without affecting the capture of the particles.

The conventional methods mentioned above are inherently random and uncontrollable, and it is difficult to accurately load a target particle. Multiple particles are often captured in the trap during one single loading process. To guarantee a certain probability of capture, one needs to spray an excessive number of samples into the air. Then the residual particle would contaminate the vacuum chamber and the optics. This makes it hard to maintain high vacuum and recapture another particle.

In recent years, new loading methods have been proposed to obtain an ultrahigh vacuum environment for optical trapping and cooling the particle. By separating a loading chamber from the experimental

chamber for cooling, one can prevent the residual particles from contaminating the vacuum chamber. Aspelmeyer's group from Universität Wien uses a science chamber and a loading chamber in the setup for a novel particle source, combining a nebulizer source with optical trapping and a hollow core photonic crystal fiber. It provides a transport mechanism capable of trapping a single nanoparticle from the nebulizer source and moving it in a controlled way into the ultrahigh vacuum (UHV) chamber, without contamination and with control over the particle number and position. Novotny's group also reported a mobile optical trap which enables cooling and long-range 3D manipulation of a silica nanoparticle in high vacuum (Mestres et al., 2015). Particles were loaded under ambient pressure in a first vacuum chamber and then transferred under vacuum into a high finesse cavity inside a second vacuum chamber. Later, they further designed a mechanical system to achieve precise long-distance transmission (20–25 cm) of nanoparticles between different chambers (Torki, 2016).

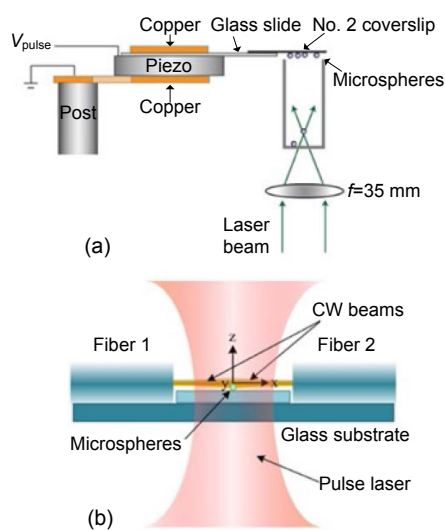


Fig. 2 Traditional launch setup with piezoelectric transducer (a) (Reprinted from Li (2013), Copyright 2013, with permission from Springer Nature) and a novel launch method with pulsed laser (b) (Reprinted from Fu et al. (2018b), Copyright 2018, with permission from Elsevier)

Rapid loading and manipulation of a microsphere in air or vacuum remains a challenge. To achieve engineering applications, a key technology is to realize an efficient and controllable loading process, in particular in the repeatable launch of the sensing

particle. The optical loading methods are more controllable than traditional methods, and we have proposed to launch and capture a single particle in a pulse-laser-assisted dual-beam fiber-optic trap (Fig. 2b), which uses pulsed optical forces to overcome the adhesion force (Fu et al., 2018a, 2018b).

3.2 Displacement detection

The measurement of displacement of trapped particles is a crucial foundation for the COM cooling of the particles and high sensitivity detection. Three detection schemes have been widely adopted: CCD detection, quadrant position detector (QPD) detection, and balanced detector plus D-shape mirror schemes.

In the CCD detection scheme, the motion state of the particle is directly extracted from the image of the CCD. The CCD imaging method is limited by the image frame rate and usually used in liquid optical tweezers or as an auxiliary means of monitoring the trapping state.

The schematic of the QPD detection scheme is shown in Fig. 3. The side scattered light is collected and collimated by the upper microscopic objective lens and received by the QPD. The motion information of the particle in the direction of the optical axis (z axis) and horizontal axis (x axis) can be obtained by the difference signal between two sets of quadrants, while the change of the total optical power indicates the motion information of the particle in the direction of the vertical axis (y axis). The QPD detection scheme has higher time resolution than an ordinary CCD camera.

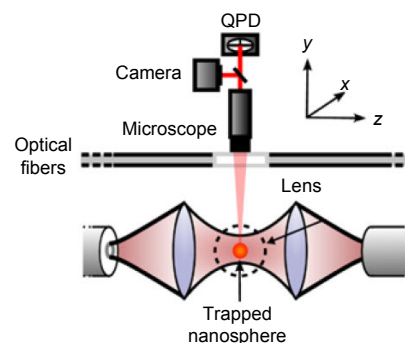


Fig. 3 Schematic of the QPD detector scheme (Reprinted from Millen et al. (2014), Copyright 2014, with permission from Springer Nature)

Fig. 4 shows the schematic of the balanced detector with the D-shape mirror scheme (Li, 2013). The

forward scattered light is separated by D-shape mirror, the sharp edge of which is perpendicular to the page for the x detector and parallel to the page for the y detector. The D-shape mirrors divide light into two parts, where their optical power is equal. Then they are focused through lens and irradiated to each photo-detector of the same type. The output voltage difference of the two photo-detectors serves as the final position signal. One detector in the z axis receives the converging light, while another receives divergent light.

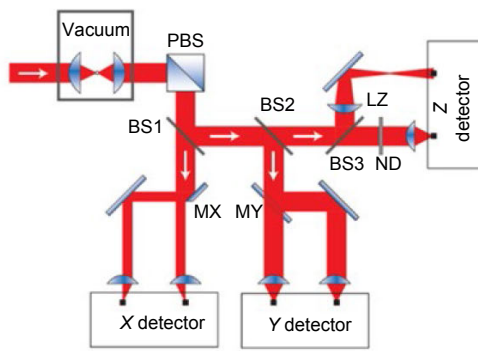


Fig. 4 Schematic of the balanced detector with the D-shape mirror scheme (Reprinted from Li (2013), Copyright 2013, with permission from Springer Nature)

The sensitive area of the photodetector used in the balanced detector is much smaller than that of the QPD, so its time resolution is better. In addition, the light intensity is enhanced by a stronger convergence in the former scheme. Thus, a higher optical signal-to-noise ratio can be acquired. The disadvantages of the balance detector are its complex structure and higher cost compared with the QPD method.

3.3 Cooling scheme

There are currently three main cooling options in vacuum optical tweezers systems: differential feedback, parametric feedback, and cavity cooling.

Differential feedback cooling applies an additional damping to the particle using the scattering force generated by the cooling laser (sometime trapping laser) (Li, 2013). In this case the PSD of the particle displacement becomes

$$S_x(\omega) = \frac{k_B T}{M \Omega^2} \frac{\Gamma_0}{\Gamma_1} \frac{\Gamma_1 \Omega^2}{(\omega^2 - \Omega^2) + \omega^2 \Gamma_1^2}, \quad (7)$$

$$\Gamma_1 = \Gamma_0 + \Gamma_{cool}$$

where Γ_{cool} is the additional damping. The RMS of the particle displacement decreases. The stiffness of the optical tweezers k is modulated according to the absolute value of the displacement of the particle in parametric feedback cooling (Vovrosh et al., 2017), and the change of PSD of the particle displacement is similar to that in differential feedback cooling. The technical difficulties of differential feedback cooling and parametric feedback cooling lie in accurate detection of the particle motion and the three-axis cooling cross heating.

Cavity cooling is based on the Doppler principle (Genes et al., 2008; Romero-Isart et al., 2011). As Fig. 5 shows, the frequency difference between cavity resonant frequency ω_c and cooling laser ω_L is exactly the free oscillation frequency of particle ω_M . Thus, the laser frequency increases to the cavity resonant frequency when the particle is moving opposite to the direction of the cooling laser and decreases to away from the cavity resonant frequency for the converse situation. Therefore, photons opposite to the direction of particle motion leak out of the cavity because they are in resonance, while photons with the same direction of particle motion are trapped in the cavity. Thus, the average of the former photons is larger than that of the latter photons. The former photons carry away energy that is from the kinetic energy of the particle. Lastly, the photons cool the vibration of the trapped microsphere.

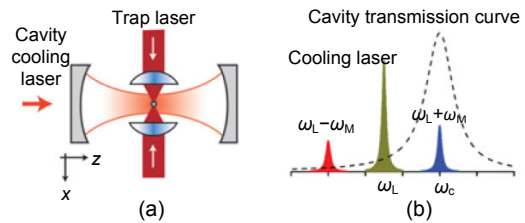


Fig. 5 Scheme of 1D cavity cooling (a) and principle of 1D cavity cooling (b) (Reprinted from Li (2013), Copyright 2013, with permission from Springer Nature)

Quantum mechanical calculations show that the steady-state phonon number of the vibration is (Barker, 2010; Chang et al., 2010)

$$\langle n_f \rangle \approx \frac{\kappa^2}{16\omega_M^2} + \frac{\gamma_{sc}}{\kappa}, \quad (8)$$

where κ is the intrinsic cavity linewidth and γ_{sc} is the

rate of a photon scattered by the particle. Quantum ground-state cooling ($\langle n_f \rangle < 1$) can be achieved when $\omega_M \gg \kappa \gg \gamma_{sc}$. Thus, cavity cooling is more suitable for use in optical tweezers with a large elastic coefficient or a cooling nanosphere rather than a microsphere, as the latter has higher requirements for the optical cavity.

In addition, the value of γ_{sc} is determined by the size of the microsphere, and some researchers suggest that ground-state cooling with a cavity should be possible for microspheres with a diameter of 1 μm or slightly larger (Yin et al., 2013) when the wavelength of the cooling laser is 1064 nm.

3.4 Diverse optical trap configurations

3.4.1 Gaussian beam trap

The particle-trapping configurations fall mainly into three groups: single beam, single beam with parabolic mirror, and counter-propagating beams (Fig. 6). To achieve higher power output and reduce the heating effect of the laser, an infrared laser is usually used for dielectric microspheres. Thus, capturing microspheres with a single beam is quite inefficient and unstable, unless using the help of gravity (upward single beam), buoyancy, or other kinds of forces. For a single beam scheme, microspheres are better trapping objects. High numerical aperture (NA) lens are necessary since single-beam capture schemes generally require a high NA lens to tightly focus the laser (Gieseler et al., 2012), and oil immersion environment is required for higher NA. When a single beam is axisymmetric and the particle is spherical, the sphere is naturally located in the center of the beam, which makes the detection components more adjustable and has higher efficiency.

In the single beam with parabolic mirror scheme, the trapping force is derived mainly from the gradient force of the backward concentrated laser of the mirror because it is tightly focused (Vovrosh et al., 2017). The scattering force of the forward parallel laser is negligible. Therefore, this scheme gives no significant increase in capture efficiency compared with a single beam scheme, and it is hard to capture microspheres stably. The advantage of this method is that a parabolic mirror has smaller aberration and the setup is robust.

When the two beams are transmitted in opposite directions, the scattering forces of both beams on the

particle become trapping forces, which improves the total capturing efficiency (Li et al., 2010). The dual-beam scheme is able to capture microspheres stably without the help of any other force. It also allows trapping particles under a lower light intensity condition and reduces the influence of the laser heating effect. When a particle is trapped in an extremely low pressure environment, the laser heats the particle with the medium and reduces the survival time of particles in optical tweezers. This method requires that the focus points of the two beams be closely coincident; otherwise, the motion of the particle will become complicated, which increases the difficulty of adjusting the beam. Table 2 lists the reported diverse optical configurations for trapping particles in vacuum.

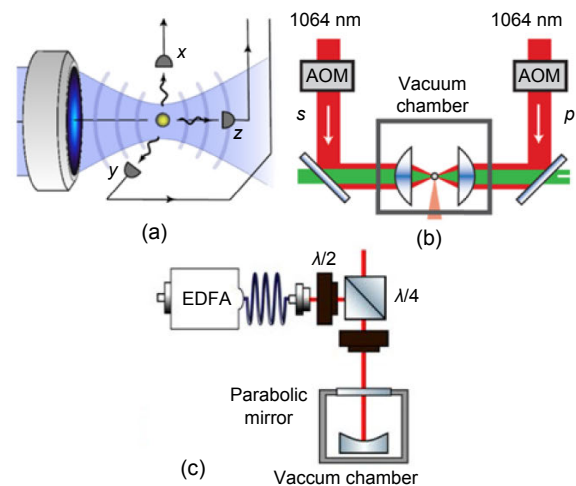


Fig. 6 Three partial optical structures, which are representative of the trapping schemes

(a) is reprinted from Gieseler et al. (2012), Copyright 2012, with permission from the American Physical Society; (b) is reprinted from Li (2013), Copyright 2013, with permission from Springer Nature; (c) is reprinted from Vovrosh et al. (2017), Copyright 2017, with permission from the corresponding author

3.4.2 Non-Gaussian beam trap

In addition to the traditional light trap, there are some unique traps with special light beams, including vortex, Laguerre-Gaussian, and Bessel. Ostrovsky et al. (2013) first introduced the concept of the “perfect vortex beam” whose intensity profile and radius remain the same regardless of topological charge. Based on these properties, a microparticle would rotate at a constant velocity if trapped with a vortex beam. Then Chen et al. proposed a novel approach

Table 2 Brief summary of diverse optical configurations

Optical configuration	Particle material & diameter	Numerical aperture	Laser & power	Cooling method	Equivalent temperature	Vacuum pressure (mbar*)	Reference
Counter-propagating incoherent beams	Silica, 3 μm	0.680	~ 50 mW per beam	Differential feedback	150, 1.5, and 68 mK for the x , y , and z modes, respectively	$5.2\text{E-}5$	Li et al. (2011)
Counter-propagating incoherent beams	Silica, 3 μm	~ 0.075	~ 120 mW per beam	Differential feedback	10, 55, and 12 K for the x , y , and z modes, respectively	$6.7\text{E-}6$	Ranjit et al. (2015)
Counter-propagating coherent beams	Silica, 300 nm	~ 0.075	~ 120 mW per beam	Differential feedback	400 mK for the one mode	$5.0\text{E-}6$	Ranjit et al. (2016)
Upward single beam	Silica, 14 μm	0.03	~ 200 mW	Differential feedback	$\sim 7/5$ mK for the x mode	$1.0\text{E-}6$	Monteiro et al. (2017)
Single beam	Silica, 140 nm	Not mentioned	Not mentioned	Parametric feedback	150, 400, and 50 mK for the x , y , and z modes, respectively	$1.0\text{E-}6$	Gieseler et al. (2012)
Single beam	Silica, 100 nm	0.9	Not mentioned	Parametric feedback	145 μK for the y mode	$6.9\text{E-}9$	Jain et al. (2016a)
Single beam	Silica, 75 nm	0.8	1064 nm ~ 100 mW	Parametric feedback	Not mentioned	$5.0\text{E-}7$	Gieseler et al. (2012)
Single beam	Silica, 177 nm	0.77	1565 nm 540 mW	No cooling	Not mentioned	$\sim 1.0\text{E-}6$	Torki (2016)
Single beam	Silica, 170 nm nanodumbbell	0.85	1550 nm 500 mW	No cooling	Not mentioned	$\sim 1.0\text{E-}4$	Ahn et al. (2018)
Single beam with parabolic mirror	Silica, 64 nm	0.995	385 mW	Parametric feedback	13, 6, and 3 mK for the x , y , and z modes, respectively	$6.0\text{E-}6$	Vovrosh et al. (2017)

* 1 mbar=100 Pa

to create a “perfect” vortex beam (Chen et al., 2013, 2014), which is meaningful for optical manipulation. Chen et al. (2015) first achieved an annular beam using an axicon and then used a spatial light modulator (SLM) to select topological charge. From the motion of the trapped particle (3- μm polystyrene spheres dispersed in heavy water), they could probe local orbital angular momentum (OAM) density and in turn improve the vortex beam (Fig. 7a). Generally, wavefront and OAM density corrections both contributed to the uniforming OAM density of the perfect vortex beam, so that the orbital angular momentum is transferred to the trapped particle in vacuum (Fig. 7b). They found that the air damping coefficient can highly affect the orbital motion of the particle as well as the beam parameter and inertial forces. Arita et al. (2017) combined “perfect vortex” and Bessel beams to form a three-dimensional potential and investigated the dynamics of the trapped microparticle. The three-dimensional photo potential well can also be inferred

from the trajectories of the trapped particle. The particle’s complex motion in the potential included rotational motion in the vortex plane and periodic orbital motion between the vortex and the Bessel beam (Fig. 7c). Here, the interaction of optical gradient forces and scattering forces with inertial forces and gravity acting on the captured particles is responsible for the motion.

4 Applications

4.1 Acceleration

Precision measurement of acceleration is crucial in inertial navigation. A levitated optomechanical system has proved to be an excellent candidate for a novel high sensitivity accelerometer. In the spring-mass oscillator model widely applicable to a variety of accelerometers, the minimum detectable acceleration purely limited by thermal noise can be expressed

as (Ranjit et al., 2015)

$$a_{\min}^{\frac{1}{2}} = \sqrt{\frac{4k_{\text{B}}T\omega_0 b}{QM}}, \quad (9)$$

where the measurement of bandwidth b is far less than the resonant frequency ω_0 . k_{B} is the Boltzmann constant and T is the ambient temperature. Q is the quality factor and M is the mass of the oscillator. Thermal noise is caused by thermal motion of the molecules around the oscillator. Q is typically limited by material loss including surface imperfections, thermo-elastic dissipation, and clamping loss in traditional macroscopic mass accelerometers. Levitating the mechanical oscillator with magnetic fields (Romero-Isart et al., 2012) or radiation pressure (Yin et al., 2013) are effective ways to avoid material loss. Trapping dielectric spheres by laser, namely optical tweezers, is one kind of representative technology. It has been applied in a fairly wide range of fields from biology (Neuman and Block, 2004) to fundamental physics (Geraci et al., 2010).

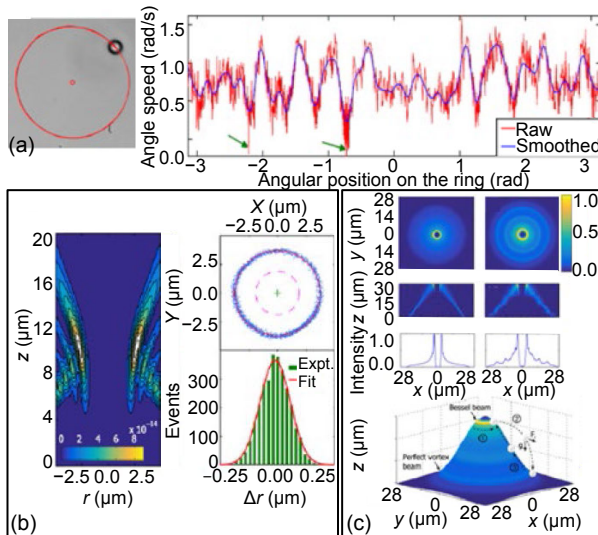


Fig. 7 Rotation analysis of a single trapped particle (a), beam profile of the LG beam and trajectories of a silica particle (b), and spatial profile of a perfect vortex beam propagating along the z axis with $l=15$ compared with numerical simulations (c)

(a) is reprinted from Chen et al. (2015), Copyright 2015, with permission from Springer Nature; (b) is reprinted from Mazilu et al. (2016), Copyright 2016, with permission from the American Physical Society; (c) is reprinted from Arita et al. (2017), Copyright 2017, with permission from the Optical Society of America

On the other hand, Eq. (9) does not consider noise resulting from physical clamping. Given that no material clamping is required plus a high vacuum environment, optical tweezers accelerometers are largely isolated from vibration noise and thermal noise, the primary noise sources for most traditional macroscopic mass accelerometers. The new additional disturbance is momentum diffusion due to photon recoil (Diehl et al., 2018), which is determined mainly by optical relative intensity noise within the scope of the mechanical motion frequency and can be controlled to a negligible level compared with noise resulting from physical clamping. Thus, although macroscopic mass accelerometers (Kapner et al., 2007) can acquire smaller acceleration sensitivities up till now, because optical tweezers employ smaller mass according to Eq. (9), optical tweezers accelerometers are still promising for higher sensitivity. Moreover, optical tweezers are special for their microscopic scale and provide an ideal tool of researching new interactions producing accelerations at distances less than $100 \mu\text{m}$ (Monteiro et al., 2017).

There are sensitivities of $7.7 \mu\text{g}/\sqrt{\text{Hz}}$ for a $d=5 \mu\text{m}$ sphere in a single beam and heterodyne detection system (Rider et al., 2018), and $47 \mu\text{g}/\sqrt{\text{Hz}}$ for a $d=3 \mu\text{m}$ sphere using a multi-beam and damp feedback scheme (Li et al., 2011). The highest acceleration sensitivity reported based on a vacuum tweezer system is $0.4 \mu\text{g}/\sqrt{\text{Hz}}$ for a $d=23 \mu\text{m}$ sphere by Monteiro (2017) in Yale University. A simplified schematic of its experimental setup is shown in Fig. 8. Microspheres are levitated using a vertical trapping beam with a small numerical aperture ($\text{NA}=0.03$) lens to decrease the efficiency of the clamping force produced by the laser, as will the elastic coefficient. The infrared laser (red in Fig. 8) used to capture the microspheres also generates feedback forces to suppress the COM motion caused by collisions with residual gas molecules. One can modulate the trapping beam for feedback in the Z direction (vertical upward direction) as defined in Fig. 8. Feedback in the X and Y directions is realized in a high-bandwidth piezo deflection mirror at frequencies up to $\sim 1 \text{ kHz}$. Two additional green beams are used to detect the motion of the microsphere in three orthogonal directions. A D-shaped mirror and balanced photodiode (BPD) are used in the X

direction to minimize detection noise. For a larger dynamic range, the motions in the Y and Z directions are imaged by lateral effect position sensors.

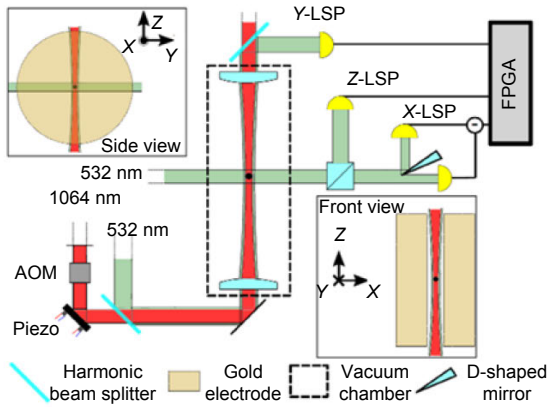


Fig. 8 Simplified schematic of the experimental setup (Reprinted from Monteiro et al. (2017), Copyright 2017, with permission from the American Physical Society)

The microspheres are surrounded by two electrodes placed in parallel. These generate the electric field for calibration. The diameter of the spheres can be inferred by the microscope images, as can the mass. One electrode is connected to a high-voltage source and another to ground. The air breaks down and becomes conducting within a strong electric field. After air discharge, the microsphere maintains its charge (Moore et al., 2014). Then an ultraviolet (UV) lamp illuminates the surface of the sphere to remove this charge by the photoelectric effect until only a net charge of a single electron is left. A weaker oscillating electric field not penetrating the air monitors the process continuously. Lastly, a factor from the detector voltage to microsphere acceleration can be acquired through a controllable and known acceleration resulting from the electric field. The above processes are also applicable to measuring sensitivity as long as the electric field is weak enough.

The trap is stable enough to sustain for month-long time scales. For the largest spheres tested, nano-g sensitivity is reached by long integrations of 10^4 s. Heating from material absorption of the laser and the efficiency of the clamping force produced by the laser limit the mass in optical tweezers. They can be both improved by finely designed materials and optical structure. The vaporization of the sphere because of laser heating also changes the density of the sphere.

The change is more severe for spheres following the Stöber chemical process than with the fused production method. The former can lead to about 10%–20% lower densities, which is the main system error of the calibration and sensitivity measurement.

In 2018, some researchers proposed the idea of resonant measurement of static gravity acceleration (Hebestreit et al., 2018). First, they trap the particle and cool its COM motion with feedback. Then both the trapping and cooling laser are turned off for a well-defined time, during which the particle leaves the trap center because of gravity. Finally, only the trap laser is turned on and the particle starts to oscillate for a while. The process essentially adds a square wave modulation to the gravitational acceleration and is expected to achieve higher sensitivity since the optical tweezer accelerometer has a higher Q value than conventional accelerometers.

4.2 Force sensor

State-of-the-art force sensitivity $12zN/\sqrt{Hz}$ has been reached in nanotube resonators in a cryogenic environment to improve their thermal-noise limited force sensitivity (Moser et al., 2013). Similar resonant solid-state mechanical sensors such as micro-cantilevers, nano-membranes, and nanotubes typically have sensitivities of $\sim 10aN/\sqrt{Hz}$ to $100aN/\sqrt{Hz}$ operated at room temperature. Their extreme force sensitivity enables the test of single-electron spins in solids (Rugar et al., 2004), the realization of sensitive chip-scale optomechanical force transducers (Miao et al., 2012), and detection for non-Newtonian gravity at sub-millimeter length scales (Geraci et al., 2008). The minimum detectable force, limited only by thermal noise, is

$$F_{\min}^{\frac{1}{2}} = \sqrt{\frac{4k_B T \omega_0 M b}{Q}}, \quad (10)$$

where the meanings of the above symbols have been explained in Eq. (9). The minimum detectable force scales with the square root of the mass. This is the reason of employing microscopic masses in resonant solid-state mechanical sensors. Macroscopic masses are used in accelerometers for the opposite principle in Eq. (9).

Applications of searching for forces that couple to mass such as gravity or the number of atoms or nucleons of the mass require optimizing the sensitivity to accelerations rather than force. Force measurement by optically levitated particles still has the advantage of no material clamping loss while forfeiting its competitiveness in the measurement scale relative to acceleration detection. Excellent environmental isolation of optically levitated particles in high vacuum can allow such systems to achieve similar or better force sensitivity at room temperature than resonant solid-state mechanical sensors (Gieseler et al., 2013).

There are sensitivities of $\sim 200 aN / \sqrt{Hz}$ for a $d=3 \mu\text{m}$ sphere in a dual-beam system (Ranjit et al., 2015), and $1.6 aN / \sqrt{Hz}$ for a $d=300 \text{ nm}$ sphere in the same trapping and feedback scheme (Ranjit et al., 2016). The latter is the smallest force sensitivity reported to date for optical tweezers, achieved by Gambhir in Nevada University in 2016. Fig. 9a shows the experimental setup. There are two equal-power counter-propagating coherent beams whose wavelengths are 1064 nm (noted with red color) used to trap the 300 nm fused silica sphere and three 532 nm laser beams for cooling the particle. In Fig. 9b, the optical force along the z axis within positions offset by $\pm 500 \mu\text{m}$ from the center has been calculated. Macroscopically, the relation curve is similar to that of counter-propagating coherent beams, while there is a standing wave consisting of many potential wells microscopically, as illustrated in the upper right corner of Fig. 9b. The distance between two adjacent potential wells is the half of the wavelength of the trapping laser. Thus, the particle will hop to an adjacent trapping site as a result of the perturbation on laser power. The above process is shown in Fig. 9c. Two advantages can be obtained from the counter-propagating coherent beam scheme. First, it can carry the particle between different potential wells, which shows possibility for sensing experiments where the position of particle must be controlled precisely (Park and Wang, 2009). Secondly, the known spacing of two adjacent potential wells also serves as a ruler to calibrate the displacement spectrum of the particle. The calibration is useful for both neutral and charged particle, so it is applicable for experiments where charge can introduce unwanted background.

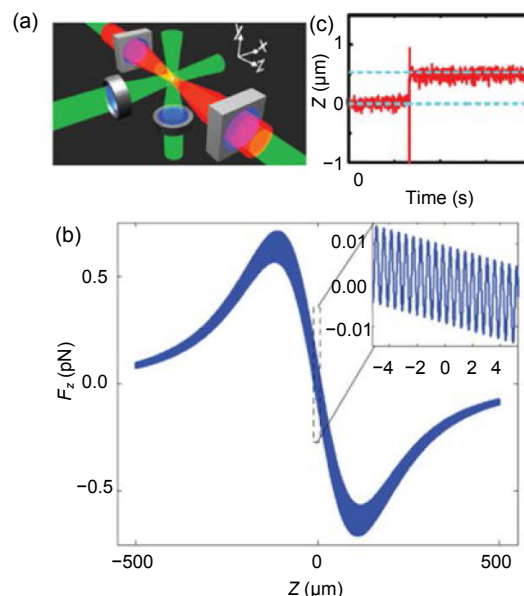


Fig. 9 Experimental setup (a), calculated optical force along the z axis (b), and time trace of particle motion in the z -axial direction (c) (Reprinted from Ranjit et al. (2016), Copyright 2016, with permission from the American Physical Society)

The COM motion of particle is cooled to 400 mK at a pressure of 6.7×10^{-9} mbar (1 mbar=100 Pa). An extremely low vacuum environment is key to such high sensitivity of microsphere motion detection. The particle can be trapped over several days, enabling a time-averaged measurement over 10^5 s and demonstrating force sensing at the $6zN$ level.

4.3 Gyroscope effect

In high vacuum, a circularly polarized laser beam can levitate and control the rotation of microspheres. Because of low damping in high vacuum, microspheres can rotate at a rate above several MHz (Arita et al., 2013). A rotation rate up to several GHz had been experimentally demonstrated. Reimann et al. from ETH reported a rotating, optically trapped silica nanoparticle in vacuum by transferring spin angular momentum of light to the particle (Reimann et al., 2018). At sufficiently low damping (at pressure 10^{-5} mbar), rotation frequencies of single 100-nm particles exceeding 1 GHz were experimentally realized. They highlight the potential application of the possibility of being used to test material limits under centrifugal stress on the nanoscale.

At almost the same time, another group led by Li TC (Ahn et al., 2018) optically levitated and rotated a 170-nm-diameter nanodumbbell with a circular polarized tightly focused single beam. The experimental scheme is shown in Fig. 10a. The COM motion, rotation, and torsional vibration can also be extracted from this single trapping beam through a different detection optical path. It is indicated that such high-speed rotation could be used to study material properties and vacuum friction.

The high-speed rotation will inevitably bring important implications to the gyroscope effect test on this scale. The external torque exerted on optically levitated systems will cause the variation of the rotation rate and precession angle on the rotating microspheres. There comes the possibility of measuring or maintaining orientation and angular velocity, namely, the gyroscope. Several groups have reported rotation frequencies up to 1 GHz (Ahn et al., 2018). The following figures show a representative experimental scheme.

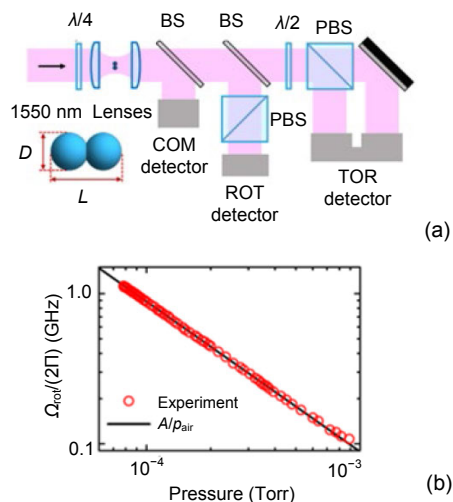


Fig. 10 Experiment scheme (a) and results (b) in Ahn et al. (2018) (Reprinted from Ahn et al. (2018), Copyright 2018, with permission from the American Physical Society)

4.4 Macroscopic quantum state

Optical levitation systems can not only be used as sensitive probes for acceleration, weak force, and tiny displacements, but also lead to possibilities of investigating the quantum behavior of macroscopic mechanical oscillators. They can shed light on understanding the quantum-to-classical transition.

In 2016, a proposal named macroscopic quantum resonators (MAQRO) was submitted in response to the “New Science Ideas” Call of the European Space Agency (ESA). The official website introduced MAQRO (<http://maqro-mission.org/>) as “a test allows probing the vastly unexplored ‘quantum-classical’ transition for increasingly massive objects, and provides unambiguous tests for so-called collapse models that have been suggested to resolve the quantum measurement problem.” It had been selected as one of three key areas of interest for further investigation in 2017 (<http://sci.esa.int/cosmic-vision/59040-esa-identifies-new-science-ideas-for-future-space-missions/>).

Quantum ground state cooling is an essential procedure for achieving a macroscopic quantum state. In a universal quantum ground state platform, an F-P cavity with an end mirror is a basic setup. Through proper setting of the cavity resonance frequency and laser frequency, the anti-Stokes process could be favored over the Stokes process. As a consequence of energy conservation, the thermal energy of the mechanical mode has to decrease to create higher-energy anti-Stokes photons. If the cavity-mode decay rate, which is related to the optical finesse, is smaller than the mechanical-mode frequency, theoretical analysis shows that these experiments can eventually achieve the quantum ground state of a macroscopic mechanical oscillator (Marquardt et al., 2007), which would be a significant breakthrough in physics from both experimental and theoretical points of view.

Many groups have experimentally demonstrated that the mechanical mode of a mechanical oscillator can be significantly cooled through optomechanical interactions (Cohadon et al., 1999; Corbitt et al., 2007; Gröblacher et al., 2008). A remarkable breakthrough was reported by Teufel (2011) and Chan (2011) (Fig. 11), in that they independently achieved 0.34 ± 0.05 and 0.85 ± 0.08 average phonon numbers, respectively, which means that the quantum ground state cooling of the nano-oscillator is realized.

Research on this type of nanomechanical system has made great strides, but this kind of system requires a huge refrigerator. In addition, currently its main challenge is the difficulty of achieving high detection efficiency due to weak coupling with the environment. The quantum interference detection through laser or microwave photons is a widely used method to improve detection efficiency, but it is not

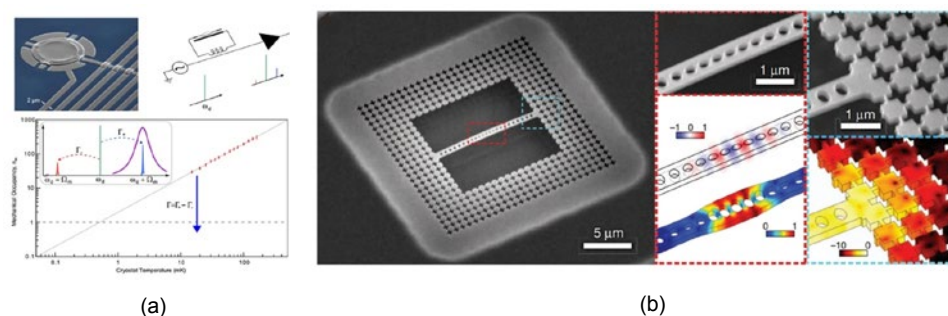


Fig. 11 Optomechanical resonators in Teufel et al. (2011) and Chan et al. (2011): (a) is reprinted from Teufel et al. (2011), Copyright 2011, with permission from Springer Nature; (b) is reprinted from Chan et al. (2011), Copyright 2011, with permission from Springer Nature

really compatible with this structure. Another kind of optical levitation resonator which uses optical tweezers in vacuum is now considered an ideal candidate for the study of macroscopic quantum effect. Its obvious advantages are: dielectric resonator levitated in space under ultrahigh vacuum pressure, eliminating the environmental noise; the resonator has interaction with the laser directly, which gives rise to high detection efficiency and ultrahigh quality factor. In this kind of system, the resonator could be cooled down to the order of micro kelvin at room temperature without the support of a pre-cooling system. Jain et al. (2016a) in ETH reported an average phonon number of 63 in an optical tweezer system in vacuum. They brought a nanoparticle into UHV (10^{-8} mbar) with active feedback and were able to realize direct measurement of photon recoil from this levitated nanoparticle. Later, they achieved an average phonon number of 21 (Jain et al., 2016b) by replacing a normal detector with a low noise, high-power photodetector capable of being a balanced photodetector of up to 70 mW of optical power.

5 Outlook

Optical tweezers, though first demonstrated nearly four decades ago, find new vitality when operating in a vacuum environment. From a force sensor to macroscopic quantum state preparation, it provides an artful platform for both fundamental physics and practical applications. The challenges of trapping single particles in vacuum have been overcome partly by the advances of laser techniques and micro manufacturing technology, but with vacuum optical tweezers there still lie many topics to be intensively

studied, for example, non-Newtonian force detection, gravitational wave detection, dark matter detection, mesoscale thermodynamics, ultrasensitive sensing, macroscopic quantum effect, and solid matter wave interferometry.

Acknowledgements

The authors acknowledge the valuable discussions with all the participants in the 2018 Hefei Symposium on Vacuum Optical Tweezers Technology and Applications.

References

- Ahn J, Xu ZJ, Bang J, et al., 2018. Optically levitated nanodumbbell torsion balance and GHz nanomechanical rotor. *Phys Rev Lett*, 121:033603. <https://doi.org/10.1103/PhysRevLett.121.033603>
- Appel J, Windpassinger PJ, Oblak D, et al., 2009. Mesoscopic atomic entanglement for precision measurements beyond the standard quantum limit. *Proc Nat Acad Sci USA*, 106(27):10960-10965. <https://doi.org/10.1073/pnas.0901550106>
- Arita Y, Mazilu M, Dholakia K, et al., 2013. Laser-induced rotation and cooling of a trapped microgyroscope in vacuum. *Nat Commun*, 4:2374. <https://doi.org/10.1038/ncomms3374>
- Arita Y, Chen MZ, Wright EM, et al., 2017. Dynamics of a levitated microparticle in vacuum trapped by a perfect vortex beam: three-dimensional motion around a complex optical potential. *J Opt Soc Am B*, 34(6):C14-C19. <https://doi.org/10.1364/JOSAB.34.000C14>
- Ashkin A, 1970. Acceleration and trapping of particles by radiation pressure. *Phys Rev Lett*, 24(4):156-159. <https://doi.org/10.1103/PhysRevLett.24.156>
- Ashkin A, 1992. Forces of a single-beam gradient laser trap on a dielectric sphere in the ray optics regime. *Biophys J*, 61(2):569-582. [https://doi.org/10.1016/S0006-3495\(92\)81860-X](https://doi.org/10.1016/S0006-3495(92)81860-X)
- Ashkin A, 2000. History of optical trapping and manipulation of small-neutral particle, atoms, and molecules. *IEEE J Sel Top Quant Electron*, 6(6):841-856.

- <https://doi.org/10.1109/2944.902132>
- Ashkin A, Dziedzic JM, 1971. Optical levitation by radiation pressure. *Appl Phys Lett*, 19(8):283-285. <https://doi.org/10.1063/1.1653919>
- Ashkin A, Dziedzic JM, 1976. Optical levitation in high vacuum. *Appl Phys Lett*, 28(6):333-335. <https://doi.org/10.1063/1.88748>
- Ashkin A, Dziedzic JM, 1977. Feedback stabilization of optically levitated particles. *Appl Phys Lett*, 30(4):202-204. <https://doi.org/10.1063/1.89335>
- Ashkin A, Dziedzic JM, Bjorkholm JE, et al., 1986. Observation of a single-beam gradient force optical trap for dielectric particles. *Opt Lett*, 11(5):288-290. <https://doi.org/10.1364/OL.11.000288>
- Ashkin A, Schütze K, Dziedzic JM, et al., 1990. Force generation of organelle transport measured *in vivo* by an infrared laser trap. *Nature*, 348(6299):346-348. <https://doi.org/10.1038/348346a0>
- Barker PF, 2010. Doppler cooling a microsphere. *Phys Rev Lett*, 105:073002. <https://doi.org/10.1103/PhysRevLett.105.073002>
- Block SM, Goldstein LSB, Schnapp BJ, 1990. Bead movement by single kinesin molecules studied with optical tweezers. *Nature*, 348(6299):348-352. <https://doi.org/10.1038/348348a0>
- Bohren CF, Huffman DR, 1983. Absorption and Scattering of Light by Small Particles. John Wiley & Sons, New York.
- Braginskii VB, Manukin AB, 1967. Ponderomotive effects of electromagnetic radiation. *Sov Phys J Exper Theor Phys*, 25(4):653-655.
- Braginskii VB, Manukin AB, Tikhonov MY, 1970. Investigation of dissipative ponderomotive effects of electromagnetic radiation. *Sov J Exp Theor Phys*, 31:829.
- Bui AAM, Stilgoe AB, Lenton ICD, et al., 2017. Theory and practice of simulation of optical tweezers. *J Quant Spectrosc Rad Transf*, 195:66-75. <https://doi.org/10.1016/j.jqsrt.2016.12.026>
- Bustamante C, Erie DA, Keller D, 1994. Biochemical and structural applications of scanning force microscopy. *Curr Opin Struct Biol*, 4(5):750-760. [https://doi.org/10.1016/S0959-440X\(94\)90175-9](https://doi.org/10.1016/S0959-440X(94)90175-9)
- Butts DLG, 2008. Development of a Light Force Accelerometer. MS Thesis, Massachusetts Institute of Technology, Massachusetts, USA.
- Callegari A, Mijalkov M, Gököz AB, et al., 2015. Computational toolbox for optical tweezers in geometrical optics. *J Opt Soc Am B*, 32:B11-B19. <https://doi.org/10.1364/JOSAB.32.000B11>
- Català F, Marsà F, Montes-Usategui M, et al., 2017. Influence of experimental parameters on the laser heating of an optical trap. *Sci Rep*, 7(1):16052. <https://doi.org/10.1038/s41598-017-15904-6>
- Chan J, Alegre TP, Safavi-Naeini AH, et al, 2011. Laser cooling of a nanomechanical oscillator into its quantum ground state. *Nature*, 478(7367):89-92. <https://doi.org/10.1038/nature10461>
- Chang DE, Regal CA, Papp SB, et al., 2010. Cavity optomechanics using an optically levitated nanosphere. *Proc Nat Acad Sci USA*, 107(3):1005-1010. <https://doi.org/10.1073/pnas.0912969107>
- Chang YR, Hsu L, Chi S, 2006. Optical trapping of a spherically symmetric sphere in the ray-optics regime: a model for optical tweezers upon cells. *Appl Opt*, 45(16):3885-3892. <https://doi.org/10.1364/AO.45.003885>
- Chen MZ, Mazilu M, Arita Y, et al., 2013. Dynamics of microparticles trapped in a perfect vortex beam. *Opt Lett*, 38(22):4919-4922. <https://doi.org/10.1364/OL.38.004919>
- Chen MZ, Mazilu M, Arita Y, et al., 2014. Optical trapping with a perfect vortex beam. In: Optical Trapping and Optical Micromanipulation XI. International Society for Optics and Photonics, 9164:91640K.
- Chen MZ, Mazilu M, Arita Y, et al., 2015. Creating and probing of a perfect vortex in situ with an optically trapped particle. *Opt Rev*, 22(1):162-165. <https://doi.org/10.1007/s10043-015-0031-7>
- Chu S, Hollberg L, Bjorkholm JE, et al., 1985. Three-dimensional viscous confinement and cooling of atoms by resonance radiation pressure. *Phys Rev Lett*, 55(1):48-51. <https://doi.org/10.1103/PhysRevLett.55.48>
- Ciminelli C, Conteduca D, Dell'Olio F, et al., 2017. Photonic, plasmonic and hybrid nanotweezers for single nanoparticle trapping and manipulation. 19th Int Conf on Transparent Optical Networks.
- Clercx HJH, Schram PPJM, 1992. Brownian particles in shear flow and harmonic potentials: a study of long-time tails. *Phys Rev A*, 46(4):1942-1950. <https://doi.org/10.1103/PhysRevA.46.1942>
- Cohadon PF, Heidmann A, Pinard M, 1999. Cooling of a mirror by radiation pressure. *Phys Rev Lett*, 83(16):3174-3177. <https://doi.org/10.1103/PhysRevLett.83.3174>
- Cohen L, 1998. The generalization of the Wiener-Khinchin theorem. Proc IEEE Int Conf on Acoustics, Speech and Signal Processing, p.1577-1580. <https://doi.org/10.1109/ICASSP.1998.681753>
- Corbitt T, Chen YB, Innerhofer E, et al., 2007. An all-optical trap for a gram-scale mirror. *Phys Rev Lett*, 98:150802. <https://doi.org/10.1103/PhysRevLett.98.150802>
- Davis KB, Mewes M, Andrews MR, et al., 1995. Bose-Einstein condensation in a gas of sodium atoms. *Phys Rev Lett*, 75(22):3969-3973. <https://doi.org/10.1103/PhysRevLett.75.3969>
- Diehl R, Hebestreit E, René R, et al., 2018. Optical levitation and feedback cooling of a nanoparticle at subwavelength distances from a membrane. *Phys Rev A*, 98(1):013851. <https://doi.org/10.1103/PhysRevA.98.013851>
- Dienerowitz M, Mazilu M, Dholakia K, et al., 2008. Optical manipulation of nanoparticles: a review. *J Nanophoton*, 2:21875. <https://doi.org/10.1117/1.2992045>
- Fu ZH, She X, Li N, et al., 2018a. A chip of pulse-laser-assisted dual-beam fiber-optic trap. Progress in Electromagnetics Research Symp, p.86-91.

- <https://doi.org/10.23919/PIERS.2018.8597625>
- Fu ZH, She X, Li N, et al., 2018b. Launch and capture of a single particle in a pulse-laser-assisted dual-beam fiber-optic trap. *Opt Commun*, 417:103-109. <https://doi.org/10.1016/j.optcom.2018.02.040>
- Genes C, Vitali D, Tombesi P, et al., 2008. Ground-state cooling of a micromechanical oscillator: comparing cold damping and cavity-assisted cooling schemes. *Phys Rev A*, 77(3):033804. <https://doi.org/10.1103/PhysRevA.77.033804>
- Geraci AA, Smullin SJ, Weld DM, et al., 2008. Improved constraints on non-Newtonian forces at 10 microns. *Phys Rev D*, 78:022002. <https://doi.org/10.1103/PhysRevD.78.022002>
- Geraci AA, Papp SB, Kitching J, 2010. Short-range force detection using optically cooled levitated microspheres. *Phys Rev Lett*, 105:101101. <https://doi.org/10.1103/PhysRevLett.105.101101>
- Gieseler J, 2014. Dynamics of Optically Levitated Nanoparticles in High Vacuum. PhD Thesis, Universitat Politècnica de Catalunya.
- Gieseler J, Deutsch B, Quidant R, et al., 2012. Subkelvin parametric feedback cooling of a laser-trapped nanoparticle. *Phys Rev Lett*, 109(10):103603. <https://doi.org/10.1103/PhysRevLett.109.103603>
- Gieseler J, Novotny L, Quidant R, 2013. Thermal nonlinearities in a nanomechanical oscillator. *Nat Phys*, 9(12):806-810. <https://doi.org/10.1038/nphys2798>
- Gong ZY, Pan YL, Videen G, et al., 2018. Optical trapping and manipulation of single particles in air: principles, technical details, and applications. *J Quant Spectrosc Rad Transf*, 214:94-119. <https://doi.org/10.1016/j.jqsrt.2018.04.027>
- Gouesbet G, 2010. T-matrix formulation and generalized Lorenz-Mie theories in spherical coordinates. *Opt Commun*, 283(4):517-521. <https://doi.org/10.1016/j.optcom.2009.10.092>
- Gouesbet G, 2019. Generalized Lorenz-Mie theories and mechanical effects of laser light, on the occasion of Arthur Ashkin's receipt on the 2018 Nobel prize in physics for his pioneering work in optical levitation and manipulation: a review. *J Quant Spectrosc Rad Transf*, 225:258-277. <https://doi.org/10.1016/j.jqsrt.2018.12.015>
- Gouesbet G, Gréhan G, 2017. Special cases of axisymmetric and Gaussian beams. In: *Generalized Lorenz-Mie Theories* (2nd Ed.). Springer, Cham, p.268-270. https://doi.org/10.1007/978-3-319-46873-0_6
- Gouesbet G, Lock JA, 2015. On the electromagnetic scattering of arbitrary shaped beams by arbitrary shaped particles: a review. *J Quant Spectrosc Rad Transf*, 162:31-49. <https://doi.org/10.1016/j.jqsrt.2014.11.017>
- Gouesbet G, Maheu B, Gréhan G, 1988. Light scattering from a sphere arbitrarily located in a Gaussian beam, using a Bromwich formulation. *J Opt Soc Am A*, 5(9):1427-1443. <https://doi.org/10.1364/JOSAA.5.001427>
- Grass D, 2013. Optical Trapping and Transport of Nanoparticles with Hollow Core Photonic Crystal Fibers. MS Thesis, University of Vienna.
- Grier DG, 2003. A revolution in optical manipulation. *Nature*, 424(6950):810-816. <https://doi.org/10.1038/nature01935>
- Gröeblacher S, Gigan S, Böehm HR, et al., 2008. Radiation-pressure self-cooling of a micromirror in a cryogenic environment. *Europhys Lett*, 81(5):54003. <https://doi.org/10.1209/0295-5075/81/54003>
- Hänsch TW, Schawlow AL, 1975. Cooling of gases by laser radiation. *Opt Commun*, 13(1):68-69. [https://doi.org/10.1016/0030-4018\(75\)90159-5](https://doi.org/10.1016/0030-4018(75)90159-5)
- Harada Y, Asakura T, 1996. Radiation forces on a dielectric sphere in the Rayleigh scattering regime. *Opt Comm*, 124(5-6):529-541. [https://doi.org/10.1016/0030-4018\(95\)00753-9](https://doi.org/10.1016/0030-4018(95)00753-9)
- Hebestreit E, Frimmer M, Reimann R, et al., 2018. Measuring gravity with optically levitated nanoparticles. *Advanced Photonics Congress*. <https://doi.org/10.1364/NOMA.2018.NoTu4J.2>
- Hoang TM, Ahn J, Bang J, et al., 2016. Electron spin control of optically levitated nanodiamonds in vacuum. *Nat Commun*, 7:12250. <https://doi.org/10.1038/ncomms12250>
- Jain V, Gieseler J, Moritz C, et al., 2016a. Direct measurement of photon recoil from a levitated nanoparticle. *Phys Rev Lett*, 116(24):243601. <https://doi.org/10.1103/PhysRevLett.116.243601>
- Jain V, Tebbenjohanns F, Novotny L, 2016b. Microkelvin control of an optically levitated nanoparticle. *Front Opt*. <https://doi.org/10.1364/FIO.2016.FF5B.2>
- Juan ML, Righini M, Quidant R, 2011. Plasmon nano-optical tweezers. *Nat Photon*, 5(6):349-356. <https://doi.org/10.1038/nphoton.2011.56>
- Kajorndejnukul V, Ding WQ, Sukhov S, et al., 2013. Linear momentum increase and negative optical forces at dielectric interface. *Nat Photon*, 7(10):787-790. <https://doi.org/10.1038/nphoton.2013.192>
- Kapner DJ, Cook TS, Adelberger EG, et al., 2007. Tests of the gravitational inverse-square law below the dark-energy length scale. *Phys Rev Lett*, 98(2):021101. <https://doi.org/10.1103/PhysRevLett.98.021101>
- Kepler J, 1619. *De cometis libelli tres, typis Andreae Apergeri, sumptibus Sebastiani Mylii bibliopolae augustani. Avgvstae Vindelicorum.*
- Kiesel N, Blaser F, Delić U, et al., 2013. Cavity cooling of an optically levitated submicron particle. *Proc Nat Acad Sci USA*, 110(35):14180-14185. <https://doi.org/10.1073/pnas.1309167110>
- Kirstine BS, Henrik F, 2004. Power spectrum analysis for optical tweezers. *Rev Sci Instrum*, 75(3):594-612. <https://doi.org/10.1063/1.1645654>
- Lebedev P 1901. Untersuchungen über die druckkräfte des lichtes. *Ann Phys*, 6:433-458 (in German).
- Lett PD, Watts RN, Westbrook CI, et al., 1988. Observation of atoms laser cooled below the Doppler limit. *Phys Rev Lett*, 61(2):169-172. <https://doi.org/10.1103/PhysRevLett.61.169>

- Li TC, 2013. Fundamental Tests of Physics with Optically Trapped Microspheres. Springer Science & Business Media, New York.
- Li TC, Kheifets S, Medellin D, et al., 2010. Measurement of the instantaneous velocity of a Brownian particle. *Science*, 328(5986):1673-1675. <https://doi.org/10.1126/science.1189403>
- Li TC, Kheifets S, Raizen MG, 2011. Millikelvin cooling of an optically trapped microsphere in vacuum. *Nat Phys*, 7(7):527-530. <https://doi.org/10.1038/nphys1952>
- Loke VLY, Nieminen TA, Heckenberg NR, et al., 2001. T-matrix calculation via discrete dipole approximation, point matching and exploiting symmetry. *J Quant Spectrosc Rad Transf*, 110(14-16):1460-1471. <https://doi.org/10.1016/j.jqsrt.2009.01.013>
- Ludlow AD, Boyd MM, Ye J, et al., 2015. Optical atomic clocks. *Rev Mod Phys*, 87(2):637-701. <https://doi.org/10.1103/RevModPhys.87.637>
- Mackowski DW, 2002. Discrete dipole moment method for calculation of the T matrix for nonspherical particles. *J Opt Soc Am A*, 19(5):881-893. <https://doi.org/10.1364/JOSAA.19.000881>
- Mao H, Arias-Gonzalez JR, Smith SB, et al, 2005. Temperature control methods in a laser tweezers system. *Biophys J*, 89(2):1308-1316. <https://doi.org/10.1529/biophysj.104.054536>
- Maragò OM, Jones PH, Gucciardi P, et al., 2013. Optical trapping and manipulation of nanostructures. *Nat Nanotechnol*, 8(11):807-819. <https://doi.org/10.1038/nnano.2013.208>
- Marquardt F, Chen JP, Clerk AA, et al., 2007. Quantum theory of cavity-assisted sideband cooling of mechanical motion. *Phys Rev Lett*, 99:093902. <https://doi.org/10.1103/PhysRevLett.99.093902>
- Mazilu M, Arita Y, Vettenburg T, et al., 2016. Orbital-angular-momentum transfer to optically levitated microparticles in vacuum. *Phys Rev A*, 94(5):053821. <https://doi.org/10.1103/PhysRevA.94.053821>
- Mestres P, Berthelot J, Spasenović M, et al., 2015. Cooling and manipulation of a levitated nanoparticle with an optical fiber trap. *Appl Phys Lett*, 107(15):151102. <https://doi.org/10.1063/1.4933180>
- Miao HX, Srinivasan K, Aksyuk V, 2012. A microelectromechanically controlled cavity optomechanical sensing system. *New J Phys*, 14:075015. <https://doi.org/10.1088/1367-2630/14/7/075015>
- Millen J, Deesuwana T, Barker P, et al., 2014. Nanoscale temperature measurements using non-equilibrium Brownian dynamics of a levitated nanosphere. *Nat Nanotechnol*, 9(6):425-429. <https://doi.org/10.1038/nnano.2014.82>
- Monteiro F, Ghosh S, Fine AG, et al., 2017. Optical levitation of 10-ng spheres with nano-g acceleration sensitivity. *Phys Rev A*, 96:063841. <https://doi.org/10.1103/PhysRevA.96.063841>
- Moore DC, Rider AD, Gratta G, 2014. Search for millicharged particles using optically levitated microspheres. *Phys Rev Lett*, 113(25):251801. <https://doi.org/10.1103/PhysRevLett.113.251801>
- Moser J, Güttinger J, Eichler A, et al., 2013. Ultrasensitive force detection with a nanotube mechanical resonator. *Nat Nanotechnol*, 8(7):493-496. <https://doi.org/10.1038/nnano.2013.97>
- Neuman KC, Block SM, 2004. Optical trapping. *Rev Sci Instrum*, 75(9):2787-2809. <https://doi.org/10.1063/1.1785844>
- Nichols EF, Hull GF, 1903. The pressure due to radiation. *Astrophys J*, 17(5):315-351. <https://doi.org/10.1086/141035>
- Nieminen TA, Rubinsztein-Dunlop H, Heckenberg NR, 2003a. Calculation of the T-matrix: general considerations and application of the point-matching method. *J Quant Spectrosc Rad Transf*, 79-80:1019-1029. [https://doi.org/10.1016/S0022-4073\(02\)00336-9](https://doi.org/10.1016/S0022-4073(02)00336-9)
- Nieminen TA, Rubinsztein-Dunlop H, Heckenberg NR, 2003b. Multipole expansion of strongly focussed laser beams. *J Quant Spectrosc Rad Transf*, 79-80:1005-1017. [https://doi.org/10.1016/S0022-4073\(02\)00335-7](https://doi.org/10.1016/S0022-4073(02)00335-7)
- Nieminen TA, Loke VLY, Stilgoe AB, et al., 2007. Optical tweezers computational toolbox. *J Opt A*, 9(8):S196-S203. <https://doi.org/10.1088/1464-4258/9/8/S12>
- Nieminen TA, Du Preez-Wilkinson N, Stilgoe AB, et al., 2014. Optical tweezers: theory and modelling. *J Quant Spectrosc Rad Transf*, 146:59-80. <https://doi.org/10.1016/j.jqsrt.2014.04.003>
- Ostrovsky AS, Rickenstorff-Parrao C, Victor A, 2013. Generation of the “perfect” optical vortex using a liquid-crystal spatial light modulator. *Opt Lett*, 38(4):534-536. <https://doi.org/10.1364/OL.38.000534>
- Park YS, Wang HL, 2009. Resolved-sideband and cryogenic cooling of an optomechanical resonator. *Nat Phys*, 5:489-493. <https://doi.org/10.1038/nphys1303>
- Peterman EJG, Gittes F, Schmidt CF, 2003. Laser-induced heating in optical traps. *Biophys J*, 84(2):1308-1316. [https://doi.org/10.1016/S0006-3495\(03\)74946-7](https://doi.org/10.1016/S0006-3495(03)74946-7)
- Peters A, Chung KY, Chu S, 2001. High-precision gravity measurements using atom interferometry. *Metrologia*, 38(1):25-61. <https://doi.org/10.1088/0026-1394/38/1/4>
- Polimeno P, Magazzù A, Iati MA, et al., 2018. Optical tweezers and their applications. *J Quant Spectrosc Rad Transf*, 218:131-150. <https://doi.org/10.1016/j.jqsrt.2018.07.013>
- Ranjit G, Atherton DP, Stutz JH, et al., 2015. Attonewton force detection using microspheres in a dual-beam optical trap in high vacuum. *Phys Rev A*, 91(5):051805. <https://doi.org/10.1103/PhysRevA.91.051805>
- Ranjit G, Cunningham M, Casey K, et al., 2016. Zeptonewton force sensing with nanospheres in an optical lattice. *Phys Rev A*, 93(5):053801. <https://doi.org/10.1103/PhysRevA.93.053801>
- Reimann R, Doderer M, Hebestreit E, et al., 2018. GHz rotation of an optically trapped nanoparticle in vacuum. *Phys Rev Lett*, 121(3):033602. <https://doi.org/10.1103/PhysRevLett.121.033602>

- Ren KF, Gréhan G, Gouesbet G, 1996. Prediction of reverse radiation pressure by generalized Lorenz-Mie theory. *Appl Opt*, 35(15):2702-2710. <https://doi.org/10.1364/AO.35.002702>
- Rider AD, Blakemore CP, Gratta GG, et al., 2018. Single-beam dielectric-microsphere trapping with optical heterodyne detection. *Phys Rev A*, 97:013842. <https://doi.org/10.1103/PhysRevA.97.013842>
- Rocheleau T, Ndikum T, Macklin C, et al., 2010. Preparation and detection of a mechanical resonator near the ground state of motion. *Nature*, 463(7277):72-75. <https://doi.org/10.1038/nature08681>
- Romero-Isart O, Pflanzner AC, Juan ML, et al., 2011. Optically levitating dielectrics in the quantum regime: theory and protocols. *Phys Rev A*, 83:013803. <https://doi.org/10.1103/PhysRevA.83.013803>
- Romero-Isart O, Clemente L, Navau C, et al., 2012. Quantum magnetomechanics with levitating superconducting microspheres. *Phys Rev Lett*, 109(14):147205. <https://doi.org/10.1103/PhysRevLett.109.147205>
- Rugar D, Budakian R, Mamin HJ, et al., 2004. Single spin detection by magnetic resonance force microscopy. *Nature*, 430(6997):329-332. <https://doi.org/10.1038/nature02658>
- Skelton SE, Sergides M, Memoli G, et al., 2012. Trapping and deformation of microbubbles in a dual-beam fibre-optic trap. *J Opt*, 14(7):075706. <https://doi.org/10.1088/2040-8978/14/7/075706>
- Sukhov S, Dogariu A, 2017. Non-conservative optical forces. *Rep Prog Phys*, 80(11):112001. <https://doi.org/10.1088/1361-6633/aa834e>
- Summers MD, Burnham DR, McGloin D, 2008. Trapping solid aerosols with optical tweezers: a comparison between gas and liquid phase optical traps. *Opt Expr*, 16(11):7739-7747. <https://doi.org/10.1364/OE.16.007739>
- Swartzlander GA Jr, Peterson TJ, Artusio-Glimpse A, et al., 2010. Stable optical lift. *Nat Photon*, 5(1):48-51. <https://doi.org/10.1038/nphoton.2010.266>
- Teufel JD, Donner T, Li DL, et al., 2011. Sideband cooling of micromechanical motion to the quantum ground state. *Nature*, 475(7356):359-363. <https://doi.org/10.1038/nature10261>
- Torki A, 2016. Mechanical Transfer of Optically Trapped Nanoparticle. MS Thesis, KTH Royal Institute of Technology.
- Townes CH, 1999. How the Laser Happened: Adventures of a Scientist. Oxford University Press, New York
- Vovrosh J, Rashid M, Hempston D, et al., 2017. Parametric feedback cooling of levitated optomechanics in a parabolic mirror trap. *J Opt Soc Am B*, 34(7):1421-1428. <https://doi.org/10.1364/JOSAB.34.001421>
- Waterman PC, 1965. Matrix for mulation of electromagnetic scattering. *Proc IEEE*, 53(8):805-812. <https://doi.org/10.1109/PROC.1965.4058>
- Waterman PC, 1971. Symmetry, unitarity, and geometry in electromagnetic scattering. *Phys Rev D*, 3:825-839. <https://doi.org/10.1103/PhysRevD.3.825>
- White DA, 2000. Numerical modeling of optical gradient traps using the vector finite element method. *J Comput Phys*, 159:13-37. <https://doi.org/10.1006/jcph.2000.6422>
- Wineland DJ, Dehmelt H, 1975. Proposed $10^{14}\Delta\nu < \nu$ laser fluorescence spectroscopy on Ti^+ mono-ion oscillator. *Am Phys Soc*, 20:637.
- Wright WH, Sonek GJ, Berns MW, 1994. Parametric study of the forces on microspheres held by optical tweezers. *Appl Opt*, 33(9):1735-1748. <https://doi.org/10.1364/AO.33.001735>
- Yin ZQ, Geraci AA, Li TC, 2013. Optomechanics of levitated dielectric particles. *Int J Mod Phys B*, 27(26):1330018. <https://doi.org/10.1142/S0217979213300181>